Middle-East Journal of Scientific Research 20 (11): 1534-1540, 2014
ISSN 1990-9233

DOI: 10.5829/idosi.mejsr.2014.20.11.114130

A Novel Method of Hysteresis Direct Torque Control of Single-Phase Induction Motor Drives

S. Ramamoorthy

Bharath University, Chennai-73, India

Abstract: This paper investigates the principle of direct torque control when applied to single-phase induction motor drive. The presented direct torque control is based on hysteresis band strategy. The proposed control scheme utilizes voltage source inverter consists of a single-phase rectifier cascaded with a four-switch inverter that provides nine voltage vectors and divided the *dq* plane into eight sectors. A modified switching pattern will be discussed to improve the performance of the drive. Simulation results are provided to illustrate the system operation. A comparison between the presented scheme and another direct torque control drive scheme will be held.

Key words: Direct torque control % Single-phase induction motor % Hysteresis comparator

INTRODUCTION

FOR a large number of years, most of the high performance techniques of induction motor drives that are widely used in industry were restricted to three-phase machines. However, many of them can be modified in order to be valid for single-phase induction motor drives that are the most utilized machines in the domestic and fractional horsepower applications. Thus, a modern technique, Direct torque and flux control (DTFC), that precisely controls this popular machine is investigated in this paper [1].

In general, single-phase machine can be viewed as a two-phase machine (main and auxiliary windings), since these windings are orthogonal in space and usually have different impedances. The most common types of such motors are the split-phase, capacitor-start, capacitor-run and capacitor-start capacitor-run. These types may need mechanical centrifugal switches to cut out the startup capacitors. In the presented control technique, all of these capacitors and centrifugal switches will be removed. Many papers have investigated different control techniques for single-phase induction motor drives. In [2] the capacitance (dc capacitor is inserted in series with the auxiliary winding of the single-phase machine) can be controlled by controlling the switching of a transistor *H* bridge in order improve the performance of the machine. The constant *V/f* strategy has been applied to control a four-switch inverter feeds the single-phase machine in [3]. Field-oriented control and vector control are also suitable to be applied to single-phase machine drives; rotor-flux-oriented control of a single-phase induction motor drive has been presented in [4]. The disadvantage of such methods is their need to a speed encoder; hence, the costs will be high if it is compared with the price of the motor itself. Recently, Neves *et al*.[5] have presented direct torque control (DTC) technique to control single-phase machine drives that is a promising strategy. Neves has presented two methods of DTC; hysteresis DTC and Field oriented DTC [9].

In this paper, a modified hysteresis DTC scheme with a modified voltage source inverter-switching pattern will be investigated[10]. As in most DTC three-phase drives, no current controllers neither the speed nor the position is necessary for the torque and flux control. Thus, a significant reduction in drive cost will take place[11].

The proposed VSI configuration shown in Fig. 1 with the modified switching patters will provide eight active switching states (voltage vectors) and one zero-voltage vector; this will divide the *dq* plan into eight sectors[12].

Single-phase Induction Machine Model: The mathematical model that describes the dynamic and the electric behaviors of single-phase induction motors can be summaries in the following equations:

Corresponding Author: S. Ramamoorthy, Bharath University, Chennai-73, India.

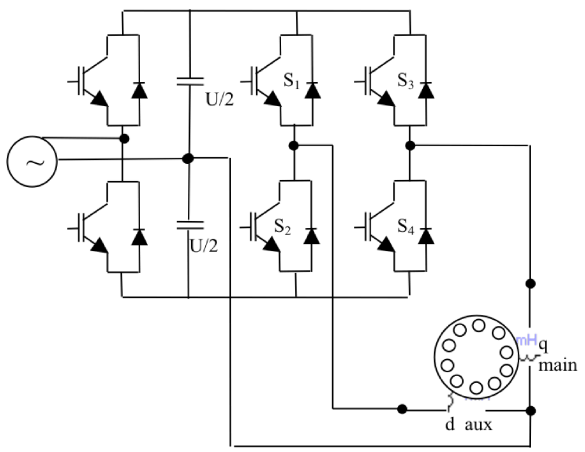

Fig. 1: Single-phase induction motor drive system

where $<_{qs}$, $<_{ds}$, i_{qs}, i_{ds}, i_{qr}, i_{dr}, 8_{ds}, 8_{ds}, 8_{qr} and 8_{dr} are the *dq*-axes voltages, currents and fluxes of the stator and rotor in the stator reference frame, r_{dq}, r_{ds} and r_r denote the stator and rotor resistances, L_{qs}, L_{ds}, L_r and L_{qm} denote the stator and the rotor self- and mutual inductances, T_r, T_e and T_L are the machine (electrical) speed and the electromagnetic and load torque and *P*, *J* and $ are the machine poles, the inertia and the viscous friction coefficient.

Notice the primed symbols mean that their measured values are referred to stator q-axis quantities according to the effective turns ratio of the windings; e.g. , $v'_{ds} = (N_{qs}/N_{ds})v_{ds}$, $i'_{ds} = (N_{ds}/N_{qs})i_{ds}$ $r'_r = (N_{qs}/N_r)^2 r_r$, …etc. where N_{qs}, N_{ds} and N_r are the stator and rotor effective number of turns [1].

$$v_{qs} = r_{qs} i_{qs} + \frac{d\, l_{qs}}{dt} \tag{1}$$

$$v'_{ds} = r'_{ds} i'_{ds} + \frac{d\, l'_{ds}}{dt} \tag{2}$$

$$0 = r'_r i'_{qr} + \frac{d\, l'_{qr}}{dt} + w_r\, l'_{dr} \tag{3}$$

$$0 = r'_r i'_{dr} + \frac{d\, l'_{dr}}{dt} - w_r\, l'_{qr} \tag{4}$$

$$l_{qs} = L_{qs} i_{qs} + L_{qm} i'_{ds} \tag{5}$$

$$l'_{ds} = L'_{ds} i'_{ds} + L_{qm} i_{qs} \tag{6}$$

$$l'_{qr} = L_{qm} i_{qs} + L'_r i'_{qr} \tag{7}$$

$$l'_{dr} = L_{qm} i'_{ds} + L'_r i'_{dr} \tag{8}$$

$$T_e = \frac{P L_{qm}}{2 L'_r} (l'_{qr} i'_{dr} - l'_{dr} i'_{qr}) \tag{9}$$

$$\frac{P}{2}(T_e - T_L) = J \frac{dw_r}{dt} + b w_r \tag{10}$$

Direct Torque Control Principle: The basic principle of the DTC is presented as follows. The instantaneous electromagnetic torque is proportional to the cross-vectorial product of the flux- linkage space vector and the stator-current space vector [6, 7]. This can be represented mathematically in equation (11)

$$T_e = C_1 \bar{l}_s \times \bar{i}_s \tag{11}$$

Equation (11) can be rewritten in the following from:

$$T_e = C_2 \,|\, \bar{l}_r \,\|\, \bar{l}_s \,|\, \sin g \tag{12}$$

where $\bar{i}_s, \bar{l}_s, \bar{l}_r$ are the stator current space vector, stator and rotor flux-linkage space vectors, respectively, $($ is the torque angle (the phase shift between the stator and rotor flux-linkage space vectors), C_1, C_2 are constants that depend upon the machine parameters (*i.e.* number of poles, self and mutual inductances).

Equations (1) and (2) can be rewritten in a vector form as:

$$\bar{v}_s = r_s \bar{i}_s + d\,\bar{l}_s / dt \tag{13}$$

Where $\bar{v}_s = v_{qs} + j v_{ds}$ is the stator voltage space vector. For simplicity, assume the stator ohmic drops to be neglected, then:

$$\bar{v}_s \approx d\,\bar{l}_s / dt \tag{14}$$

$$\Delta \bar{l}_s \approx \bar{v}_s \Delta t \tag{15}$$

It can be seen that the inverter output voltage ($\bar{v}_s = \hat{u}_i$, I= 0, 1, 2,…8), Fig. 2, directly impresses the stator flux, thus the required stator-flux locus will be obtained by using the appropriate inverter voltages (obtained by using the appropriate inverter switching states). It will be discussed below, how that comes true. It follows from (15) that in a short time)t, when the voltage vector is applied, $\Delta \bar{l}_s \approx \bar{v}_s \Delta t$. Thus the stator flux-linkage space vector moves by $\bar{l}_s$, in a trajectory parallel to the direction of the applied stator-voltage space vector (which is proportional to the D.C. link voltage). More details about the inverter voltage vectors will be discussed in the section IV.

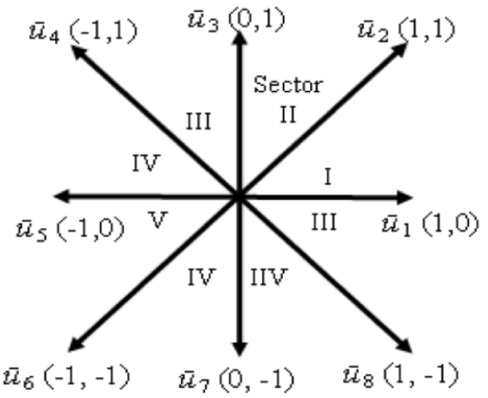

Fig. 2: Voltage vectors in single-phase inverter output.

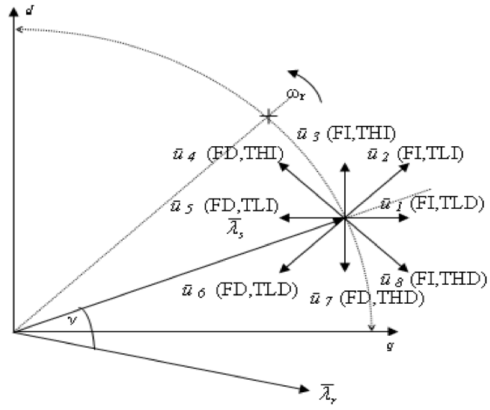

Fig. 3: Position of stator flux-linkage space-vector and selection of optimum switching voltage vector.

The goal of the DTC principle is to control directly the magnitude of both of the developed torque and the stator flux linkage of the induction motor separately. It follows from (15) and Fig. 3 that $\bar{v}_s$ can directly change both of the magnitude and the rotating speed of $\bar{l}_s$. Torque control can be made easier by keeping the magnitude of $\bar{l}_s$ constant in DTC, which in turn ensures that $\bar{l}_r$ to remain constant as well. Therefore the motor instantaneous torque will directly change with the variation of the torque angle δ only, which is affected by the relative movement of $\bar{l}_s$ and $\bar{l}_r$. In Fig. 3, if the magnitude of the measured stator flux linkage $\bar{l}_s$ is greater than the given flux reference l_s^* while it lays in sector 1, for instance, a voltage vector that forces $\bar{l}_s$ to decrease is selected such as $\bar{u}_4,\bar{u}_5,\bar{u}_6$ or $\bar{u}_7$. On the other hand, if l_s is greater than l_s^*, a voltage vector that impose l_s to increase is exerted such as $\bar{u}_2,\bar{u}_3,\bar{u}_1,$ or $\bar{u}_8$. Using a similar manner in each sector ensures that the l_s will be controlled within a pre-specified band.

Voltage Source Inverter Construction: The VSI configuration shown in Fig. 1 can provide eight non-zero active voltage-switching vectors ($\hat{u}_1$-$\hat{u}_8$) and one zero space vector $\hat{u}_0$, as shown in Fig. 2. As it is shown in Fig. 1, each limb of the two-limb inverter has two power switches, each switch has two states (*ON=1* or *OFF=0*). Hence, there are three possible switching modes; the three possible switching modes of the first limb for example are, $S_1=1$ and $S_2=0$, $S_1=0$ and $S_2=1$, or $S_1=0$ and $S_2=0$. Of course, the case at which both of the switches S_1 and S_2 are *ON* simultaneously is refused to avoid short circuit on the dc link to take place. Hence, the total possible switching states (voltage vectors) of the proposed inverter is 3^2=9 states, where 3 is the number of the possible modes per limb and 2 is the number of limbs of the inverter. This VSI switching-pattern will divide the stator-voltage space into eight sectors; each sector covers forty-five electrical degrees.

The switching pattern that is utilized in the hysteresis DTC drive presented in [5] provides four active switching states only and divides the stator-voltage space into four sectors; each sector covers ninety electrical degrees. This pattern causes a problem when the stator flux vector is near the border of a sector; the voltage vector component in quadrature with the flux vector may be too small to give the desired result of reducing the torque error and the technique may fail [5]. This problem does not exist in the DTC technique presented in this paper. There are eight active voltage vectors available and the *dq* plane is divided into eight sectors. Thus, the possibility of choosing a voltage vector for flux and torque correction that is at least 45 degrees apart from the stator flux vector at the border of the sector.

The most important feature of the presented switching pattern is the redundancy of the voltage vectors; this greatly improves the performance; increases the torque response and reduce the torque and flux ripples, as it will be shown later [8].

Switching Lookup Table: In this section, the algorithm of selecting the voltage vector which controls both torque and flux simultaneously is described. Under the condition of flux magnitude being kept at a given value, according to (12) the torque can be controlled by changing the torque angle δ. Suppose the rotor flux $\bar{l}_r$ lags the stator flux $\bar{l}_s$ by a certain angle δ as depicted in Fig. 3. From (15) one can see that rotating speed of δ is directly determined by the selected voltage vector. Hence rapid change in the developed torque can be obtained by altering the rotating speed of δ. Thus, if a torque increase is required, δ has to

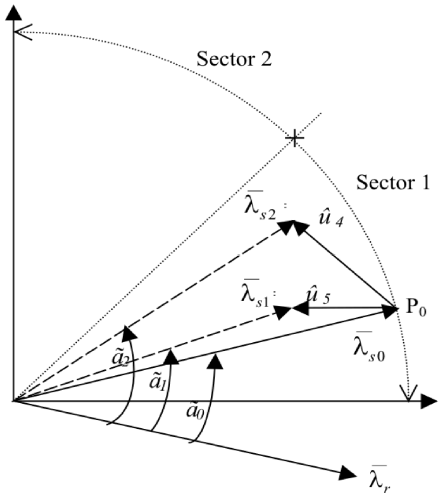

Fig. 4: Effect of the selected voltage vectors on advancing the angle of the stator flux-linkage space vector δ_s and torque angle ρ.

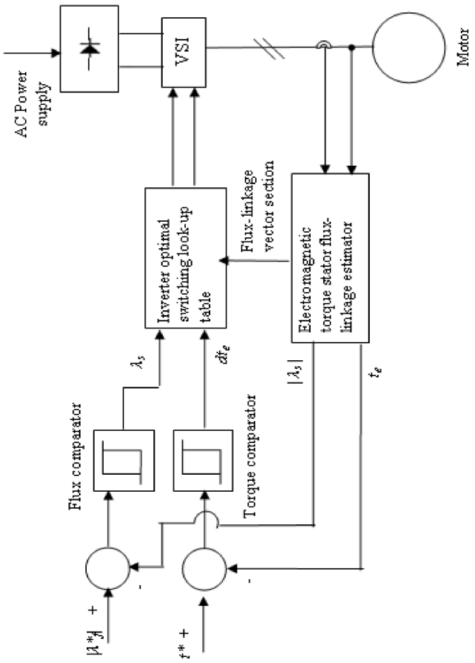

Fig. 5: Block schematic of direct torque and flux controlled single-phase induction motor drive.

be enlarged and vice versa. Referring to the same example of which l_s lays in sector 1 as seen in Fig. 3, it can be seen that, applying $\bar{u}_2$ or $\bar{u}_3$ will result in enlarging ρ while l_s will be increased as will, $\bar{u}_4$ or $\bar{u}_5$ enlarges ρ and decreases l_s, $\bar{u}_1$ or $\bar{u}_8$ reduces ρ ($\bar{l}_s$ will be forced to move towards $\bar{l}_r$) and increases l_s and finally $\bar{u}_6$ or $\bar{u}_7$ reduces ρ and decreases l_s. Another method to decrease the torque (i.e. to reduce ρ) is to apply a zero voltage vector; this will stop $\bar{l}_s$ rotating while letting $\bar{l}_r$ keep going.

Table 1: Optimal switching look-up table

$d\delta$	$d\tau_e$	*I*	*II*	*III*	*IV*	*V*	*VI*	*VII*	*VIII*
1	-2	$\hat{u}_8$	$\hat{u}_1$	$\hat{u}_2$	$\hat{u}_3$	$\hat{u}_4$	$\hat{u}_5$	$\hat{u}_6$	$\hat{u}_7$
	-1	$\hat{u}_1$	$\hat{u}_2$	$\hat{u}_3$	$\hat{u}_4$	$\hat{u}_5$	$\hat{u}_6$	$\hat{u}_7$	$\hat{u}_8$
	0	$\hat{u}_0$	$\hat{u}_0$	$\hat{u}_0$	$\hat{u}_0$	$\hat{u}_0$	$\hat{u}_0$	$\hat{u}_0$	$\hat{u}_0$
	1	$\hat{u}_2$	$\hat{u}_3$	$\hat{u}_4$	$\hat{u}_5$	$\hat{u}_6$	$\hat{u}_7$	$\hat{u}_8$	$\hat{u}_1$
	2	$\hat{u}_3$	$\hat{u}_4$	$\hat{u}_5$	$\hat{u}_6$	$\hat{u}_7$	$\hat{u}_8$	$\hat{u}_1$	$\hat{u}_2$
0	-2	$\hat{u}_7$	$\hat{u}_8$	$\hat{u}_1$	$\hat{u}_2$	$\hat{u}_3$	$\hat{u}_4$	$\hat{u}_5$	$\hat{u}_6$
	-1	$\hat{u}_6$	$\hat{u}_7$	$\hat{u}_8$	$\hat{u}_1$	$\hat{u}_2$	$\hat{u}_3$	$\hat{u}_4$	$\hat{u}_5$
	0	$\hat{u}_0$	$\hat{u}_0$	$\hat{u}_0$	$\hat{u}_0$	$\hat{u}_0$	$\hat{u}_0$	$\hat{u}_0$	$\hat{u}_0$
	1	$\hat{u}_5$	$\hat{u}_6$	$\hat{u}_7$	$\hat{u}_8$	$\hat{u}_1$	$\hat{u}_2$	$\hat{u}_3$	$\hat{u}_4$
	2	$\hat{u}_4$	$\hat{u}_5$	$\hat{u}_6$	$\hat{u}_7$	$\hat{u}_8$	$\hat{u}_1$	$\hat{u}_2$	$\hat{u}_3$

Fig. 4 shows, according to the previous example, the effect of selecting two different voltage vectors on the torque angle. Suppose $\bar{l}_{s0}$ is the flux-linkage vector which was originally located at P_0, if it is required to increase the torque and decrease the flux for instance, $\bar{u}_4$ or $\bar{u}_5$ will be adequate to be used; any of the new torque angles ρ_2 or ρ_1 will be greater than the original one ρ_0 (*i.e.* torque increase will take place). But as ρ_2 is greater than ρ_1, the rotating speed of $\bar{u}_5$ in case of using $\bar{u}_4$ will be faster than that of its value in case of applying $\bar{u}_5$ for the same period of time. Thus, if a high torque response is required $\bar{u}_4$ will be efficient than $\bar{u}_5$ and vice versa. This can be seen clear in Fig. 3, where *FI* stands for flux increase; *FD*: flux decrease; THI: torque high increase; *TLI*: torque low increase; *THD*: torque high decrease; *TLD*. In summary, by selecting the proper voltage vector both the flux and torque could be directly controlled at their given values [13]. This can be summarized in a switching look-up table, as seen in Table 1.

Proposed DTC Scheme: Fig. 5 shows the overall block diagram of the proposed direct torque control of single-phase induction motor drive [14]. As shown in Fig. 6 (a), the flux comparator is a simple hysteresis comparator. If a stator flux-linkage increase is required then $d\delta = 1$; if a stator flux-linkage decrease is required then $d\delta = 0$. The notation corresponds to the fact that the digital outputs required, then $d\tau_e = 2$. If a low torque increase is required then $d\tau_e = 1$. If a high torque decrease is required, then $d\tau_e = -2$. If a low torque decrease is required, then $d\tau_e = -1$. If no change in the torque is required then $d\tau_e = 0$. The notation corresponds to the fact that the output signals of a five-level (four loops) hysteresis comparator are $d\tau_e$, produce signals of a two-level (one loop) hysteresis comparator are $d\delta$. In the same manner for the torque comparator, as seen in Fig. 6 (b), If a high torque increase.

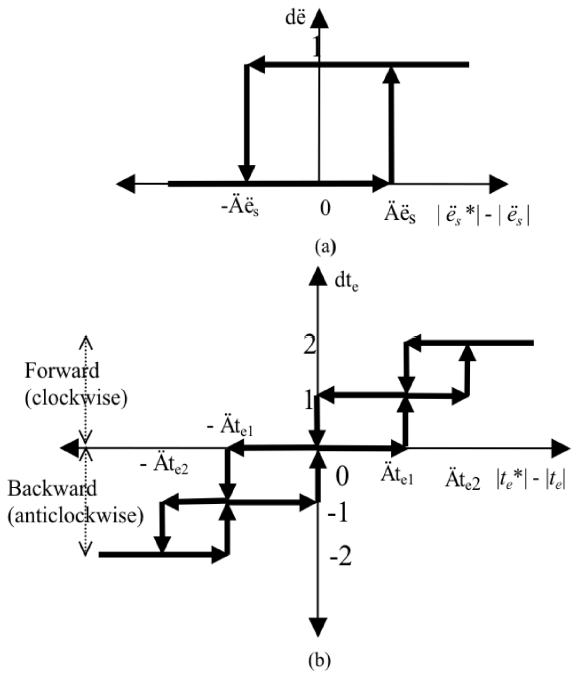

Fig. 6: (a) Two-level (one loop) Flux hysteresis comparator, (b) Five-level (four-loop) Torque hysteresis comparator.

The optimum switching look-up table requires knowledge of the position of the stator flux-linkage space-vector; since it must be determined at which sector the stator flux-linkage space-vector is located.

Since $\bar{l}_s = |\bar{l}_s| \exp(j r_s) = l_{sq} + j l_{sd}$, according to Fig. 2, the location of $\bar{l}_s$ can be determined according to the following algorithm:

if δ_{sq}>0 and δ_{sd} >0 then
 if $|\delta_{sq}| > |\delta_{sd}|$then " = "(2) else " = "(1)
elseif δ_{sq}>0 and δ_{sd} <0 then
 if $|\delta_{sq}| > |\delta_{sd}|$then " = "(7) else " = "(8)
elseif δ_{sq}<0 and δ_{sd} <0 then
 if $|\delta_{sq}| > |\delta_{sd}|$then " = "(6) else " = "(5)
 elseif $|\delta_{sq}| > |\delta_{sd}|$then " = "(3) else " = "(4).

It is worthy to note that, the quadrature and direct components of the stator flux linkages δ_{sq} and δ_{sd} are estimated using equations (1) and (2):

$$l_{sq} = \int (v_{sq} - r_{sq} i_{sq}) dt \quad (16)$$

$$l_{sd} = \int (v_{sd} - r_{sd} i_{sd}) dt \quad (17)$$

RESULTS

Torque, flux, stator currents were investigated with the help of a strong simulation tool (Simulink 4.0, in Matlab 6.0 (R12), MathWorks, Inc.) to verify the effectiveness of the proposed drive. The electrical and mechanical parameters of the single-phase induction motor that is used in the simulations are given in the appendix.

Fig. 7 shows the DTC drive response when the drive starts-up from rest (*i.e.* no initial magnetic flux). This figure shows that, the developed electromagnetic torque rises from zero to 1N.m. and settles within its pre-specified hyesteresis band in 8ms. In the same manner, stator flux was initially zero then rises to 0.3 Wb within 16ms. Fig. 8 shows the stator currents at start-up. It can be seen from this figure that high current values reach about 300% are initially imposed in order to produce the magnetic flux. Such high currents disappear as soon as the flux reaches the reference value [14].

Fig. 9 shows the stator flux trajectory of the controlled motor using the DTC drive. It can be seen from that figure that the flux trajectory is a perfect circular path. This contrasts with the usual stator flux trajectory of single-phase induction motors which is usually sharp due to the windings asymmetry.

In Fig. 10, the proposed DTC drive has been commanded to follow the torque reference at different operating points while flux reference is maintained at 0.4Wb. Torque commands of 0N.m, 1N.m, -1N.m and 0.5N.m at t = 0s, 0.2s, 0.4s and 0.6s, respectively, are applied. This figure shows the high torque response of the proposed DTC drive. Fig. 11 shows the corresponding stator currents.

Fig. 12 shows torque and flux zoom in around t =0.4 it can be seen that, the torque command has been changed from 1N.m to -1N.m, the electromagnetic torque follows the torque reference within about 250ìs, while the stator flux has maintained within its hysteresis band (i.e. each of torque and flux is decoupled completely).

For the purpose of comparing the response of the proposed DTC scheme with that has been presented in [4] at which another hysteresis DTC drive its VSI provides only four voltage vectors and divides the *dq* plan into four sectors only. Fig. 13 is taken from [4] and shows the response of the DTC drive presented by Neves. It can be seen that, for the same torque and flux commands that were presented in Fig. 10, in Fig. 10 the torque ripples

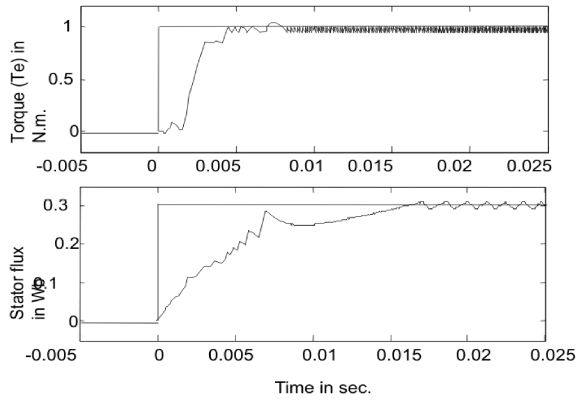

Fig. 7: Torque (N.m) and flux (Wb) responses of the proposed hysteresis DTC scheme at start-up.

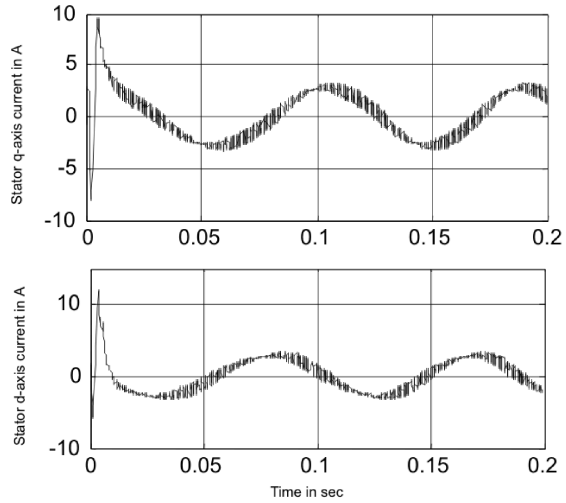

Fig. 8: Stator currents at start-up.

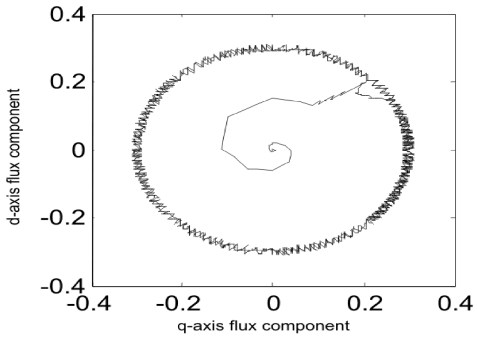

Fig. 9: Stator flux trajectory of DTC drive; its magnitude is set at 0.3 Wb.

(noise) is greatly reduced from about 42 % of rated torque in case of Neves' model [4] to about 10 % in case of this work due to the redundant stator-voltage space-vectors which can be provided by the VSI and PWM configuration.

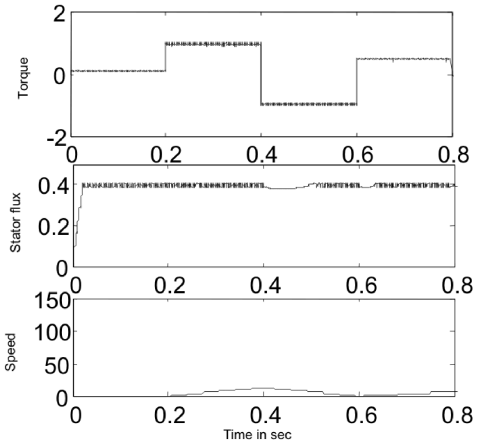

Fig. 10: Torque (N.m), Stator flux (Wb) and speed (rad/se).

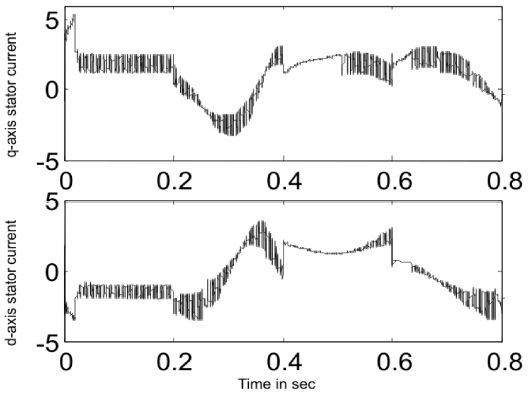

Fig. 11: Stator currents of the DTC drive in (A) during the different torque commands.

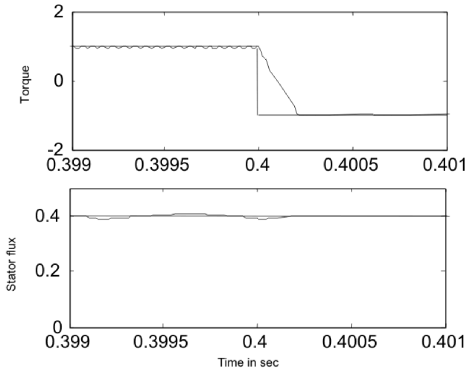

Fig. 12: Torque and flux zoom in at time t = 0.4 s.

CONCLUSIONS

In this paper, a direct torque controlled drive of single-phase induction motors has been presented. The proposed scheme is based on the conventional

hysteresis DTC schemes for three-phase induction motors. The proposed VSI configuration provides nine voltage-vectors and divides the *dq* plane into eight sectors. A switching lookup table is used to choose the optimal voltage-vector to control both of the stator flux-linkage and the torque separately. The proposed DTC algorithm distinguishes between low and high torque errors. The performance of the presented DTC scheme has been tested by simulation. The simulation results shows fast torque and flux responses of this method. The eight-sector scheme presented in this paper: when compared with the four-sector scheme, reduces the torque noise from about 42 % to about 10 % of the rated torque. A problem associated with the four-sector scheme has been avoided.

REFERENCES

1. Chee-Mun, O., Dynamic Simulation of Electric Machinery, Using Matlab/Simulink, Prentice Hall PTR, pp: 214-221, 243-249.
2. Lettenmaier, T.A., D.W. Novotny and T.A. Lipo, 1991. Single-Phase Induction Motor with an Electronically Controlled Capacitor, IEEE Trans. Ind. Elect., 27(1): 38-43.
3. Corrêa, M.B.R., C.B. Jacobina, A. Lima and E. Silva, 2000. Rotor-Flux-Oriented Control of a Single-Phase Induction Motor Drive, IEEE Trans. Ind. Elect., 47(4): 832-841.
4. Neves, F., R.P. Landim, E.B.S. Filho, Z.D. Lins, J.M.S. Cruz and A.G. Accioly, 2002. Single-Phase Induction Motor Drives with Direct Torque Control, in Proc. IEEE – IECON'02, 1(5/8): 241-246.
5. Takahashi, I. and T.A. Noguchi, 1986. A new quick-response and high efficiency control strategy of an induction motor, IEEE Trans. Ind. Appl. IA-22(5): 820-827.
6. Takahashi, I. and Y. Ohmori, 1989. High-Performance Direct Control of an Induction Motor, IEEE Trans. Ind. Appl., 25(2): 257-264.
7. Vas, P., 1998. Sensorless Vector and Direct Torque Control, Oxford University Press, Chapter, 4.
8. Young, C.M., C.C. Liu and C.H. Liu, 1996. New inverter-driven design and control method for two-phase induction motor drives, Proc. IEE-Elec. Power Appl., 143(6): 458-446.
9. Saravanan, T., V. Srinivasan and R. Udayakumar, 2013. A Approach for Visualization of Atherosclerosis in Coronary Artery, Middle-East Journal of Scientific Research, ISSN:1990-9233, 18(12): 1713-1717.
10. Saravanan, T., G. Saritha and R. Udayakumar, 2013, A Robust H-Infinity Two Degree of Freedom Control for Electro Magnetic Suspension System, Middle-East Journal of Scientific Research, ISSN:1990-9233, 18(12): 1827-1831.
11. Udayakumar, R., V. Khanna, T. Saravanan G. Saritha, 2013. Retinal Image Analysis Using Curvelet Transform and Multistructure Elements Morphology by Reconstruction,Middle-East Journal of Scientific Research, ISSN:1990-9233, 16(12): 1798-1800.
12. Udayakumar, R., V. Khanna, T. Saravanan, G. Saritha, 2013. Cross Layer Optimization For Wireless Network (Wimax), Middle-East Journal of Scientific Research,ISSN:1990-9233, 16(12): 1786-1789.
13. Thooyamani, K.P., V. Khanaa and R. Udayakumar, 2013. Blue tooth broad casting server, Middle-East Journal of Scientific Research, ISSN:1990-9233, 15(12): 1707-1712.
14. Thooyamani, K.P., V. Khanaa and R. Udayakumar, 2013. Weed control system of tea garden using GIS based database Management system, Middle-East Journal of Scientific Research, ISSN:1990-92331 5(12): 1702-1706.